

Top-of-atmosphere radiative cooling with white roofs: experimental verification and model-based evaluation

This article has been downloaded from IOPscience. Please scroll down to see the full text article.

2012 Environ. Res. Lett. 7 044007

(<http://iopscience.iop.org/1748-9326/7/4/044007>)

View [the table of contents for this issue](#), or go to the [journal homepage](#) for more

Download details:

IP Address: 115.248.114.242

The article was downloaded on 12/12/2012 at 05:52

Please note that [terms and conditions apply](#).

Top-of-atmosphere radiative cooling with white roofs: experimental verification and model-based evaluation

Francisco Salamanca¹, Shaheen Tonse², Surabi Menon^{1,3}, Vishal Garg⁴, Krishna P Singh⁵, Manish Naja⁶ and Marc L Fischer¹

¹ Lawrence Berkeley National Laboratory, CA, USA

² TST Scientific Consulting, CA, USA

³ ClimateWorks Foundation, CA, USA

⁴ IIT Hyderabad, India

⁵ Biophysics Unit, GB Pant University of Agriculture and Technology, Pantnagar, Uttarakhand, India

⁶ Aryabhata Research Institute of Observational Sciences (ARIES), Nainital, India

E-mail: fsalaman@asu.edu and mlfischer@lbl.gov

Received 13 August 2012

Accepted for publication 21 September 2012


Published 8 October 2012

Online at stacks.iop.org/ERL/7/044007

Abstract

We evaluate differences in clear-sky upwelling shortwave radiation reaching the top of the atmosphere in response to increasing the albedo of roof surfaces in an area of India with moderately high aerosol loading. Treated (painted white) and untreated (unpainted) roofs on two buildings in northeast India were analyzed on five cloudless days using radiometric imagery from the IKONOS satellite. Comparison of a radiative transfer model (RRTMG) and radiometric satellite observations shows good agreement ($R^2 = 0.927$). Results show a mean increase of $\sim 50 \text{ W m}^{-2}$ outgoing at the top of the atmosphere for each 0.1 increase of the albedo at the time of the observations and a strong dependence on atmospheric transmissivity.


Keywords: aerosol loading, cool roof, radiation balance, satellite radiometry, surface reflectance, urban systems, white roof

 Online supplementary data available from stacks.iop.org/ERL/7/044007/mmedia

1. Introduction

Replacement of natural surfaces by urban surfaces, the growing expansion of cropland areas and the emission of anthropogenic contaminants (trace gases, particles etc), are factors that affect the climate at local, regional and global scales. In spite of the foreseeable growing urban population predicted for the next years, human beings have the capacity to reduce the impact of their activities in the climate. In previous work, Menon *et al* (2010) used an uncoupled global land surface model to predict the increase in outgoing radiation

at the top of the atmosphere (TOA) in response to increasing surface albedo of roofs (albedo ≈ 0.25) and pavements (0.15) in tropical and temperate cities. The resulting summer (all hour) average increase in outgoing radiation was 18.2 W m^{-2} for each 0.1 increase in urban albedo over USA. Considering all urban areas globally, the emitted CO_2 offset was found to be $\sim 57 \text{ Gt CO}_2$. Further work by Millstein and Menon (2011) employed a fully coupled land-atmosphere regional climate WRF (weather research and forecasting) model to estimate the increase in annual mean outgoing radiation obtained from increasing urban albedos (roofs and pavements). Here, the researchers predicted an annual (all hour) average increase of 18.4 W m^{-2} in outgoing radiation at TOA for each 0.1 increase in urban albedo over USA, and afternoon temperature reductions (in urban locations) of $0.22 \pm 0.13 \text{ }^\circ\text{C}$ and $0.18 \pm$

 Content from this work may be used under the terms of the [Creative Commons Attribution-NonCommercial-ShareAlike 3.0 licence](http://creativecommons.org/licenses/by-nc-sa/3.0/). Any further distribution of this work must maintain attribution to the author(s) and the title of the work, journal citation and DOI.

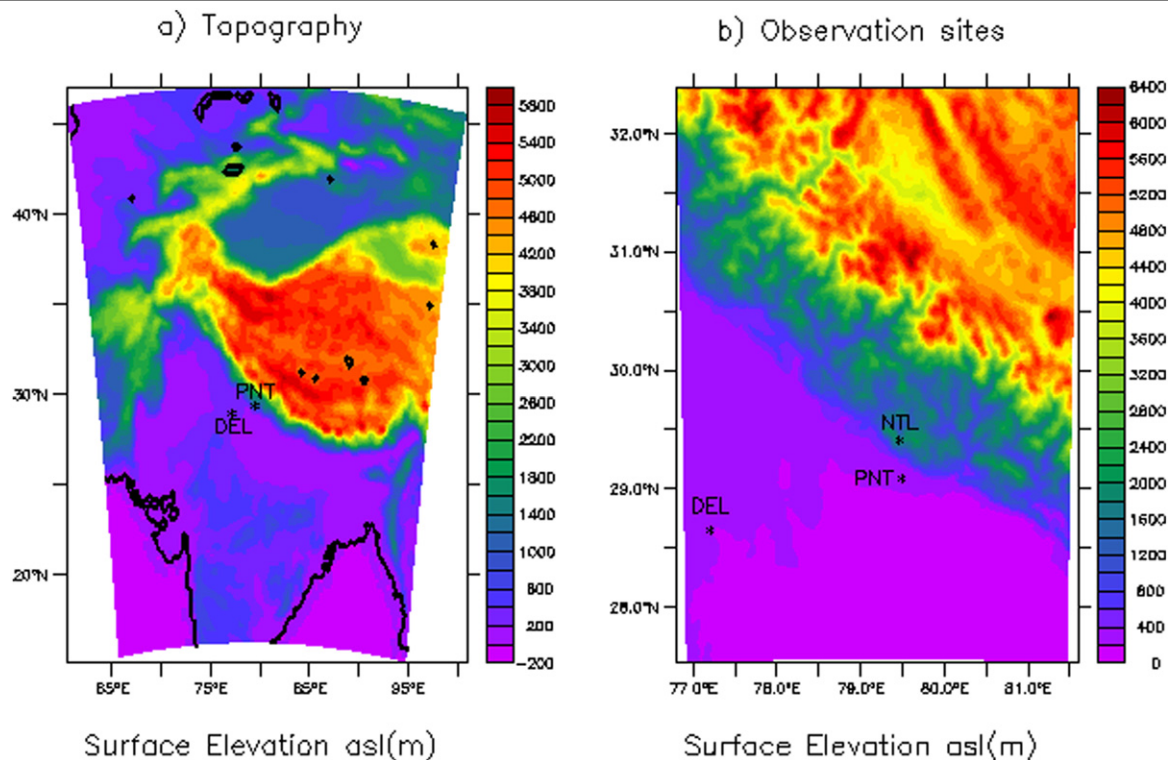


Figure 1. (a) Geographical location of Pantnagar (PNT) and New Delhi (DEL), (b) PNT, DEL and Nainital (NTL). The proximity of the Himalayan Mountains can be seen in the figures.

0.02 °C in summer and winter respectively. This suggests that the reflective cool surfaces can play a beneficial role in mitigating GHG warming by increasing the outgoing radiative fluxes at TOA, so that surface heating is reduced, thereby also reducing mean air temperature and hence energy demands for cooling in warm climates.

In this paper we experimentally evaluate the changes in radiative forcing introduced by increasing surface albedo using radiometric satellite observations from the IKONOS-2 satellite (GeoEye Inc.), and compare the results with prediction from a radiative transfer model (RRTMG_SW) (Iacono *et al* 2008). In section 2, we describe the methods used, including the field sites, ground measurements, and modeling. In section 3, we describe and discuss the results. In section 4, we conclude the paper with suggestions for further work.

2. Methods

2.1. Ground sites and measurements

Roof surfaces were modified (during spring 2011) and monitored at two locations in northern India during June 2011–March 2012. The first site was located at the GB Pant University (Pantnagar; 29.03°N, 79.49°E, 235 m asl), an agricultural and industrial area. The second site was located at the Aryabhata Research Institute of Observational Sciences (Nainital; 29.36°N, 79.46°E, ~1940 m asl), in the central Himalayan region about 30 km north of Pantnagar. Figure 1 shows the geographical location of both observation sites. The high altitude Himalayan Mountains lie in the Northern and

Eastern sectors of the second observation site and 50–130 km away. The Pantnagar university campus has a perimeter of about 30 km and encompasses a large area of about 16 000 acres (about 6.5 km²) and is used primarily for agricultural research. Local sources of aerosol and gaseous emissions near the observation location include residential cooking, diesel vehicles for the university campus and surrounding agriculture. Industrial activity is present in nearby towns. Two roofs at Pantnagar (PW1 and PW2) were painted with white elastomeric coating in June 2011. Two other roofs were left untreated (PD1 and PD2). The roof labeled PD2 could be considered to have an intermediate albedo because it was more reflective than PD1 but less reflective than PW2 and PW1. A similar strategy was followed for painted (NW1 and NW2) and unpainted (ND1 and ND2) roofs at Nainital. The painted and unpainted surface areas were similar at each site.

Four-component radiometers (Kipp and Zonnen NR01) were deployed on the four roofs at each of the two sites to measure shortwave $SW\uparrow_{SFC}$ and longwave upwelling $LW\uparrow_{SFC}$, and shortwave $SW\downarrow_{SFC}$ and longwave downwelling $LW\downarrow_{SFC}$ ground fluxes. SW surface albedo was computed as the ratio $SW\uparrow_{SFC}/SW\downarrow_{SFC}$. All the variables were measured every 10 s, and then averaged with 30 min resolution and reported here for the period from October 2011 to March 2012. Mean downwelling radiation and measurement error for each site and time period were estimated using the data from the four replicate radiometers.

2.2. Satellite measurements of $SW\uparrow_{TOA}$ radiation

Roofs were imaged using the IKONOS-2 satellite (IKO1 1999). Six satellite images of the instrumented rooftops at

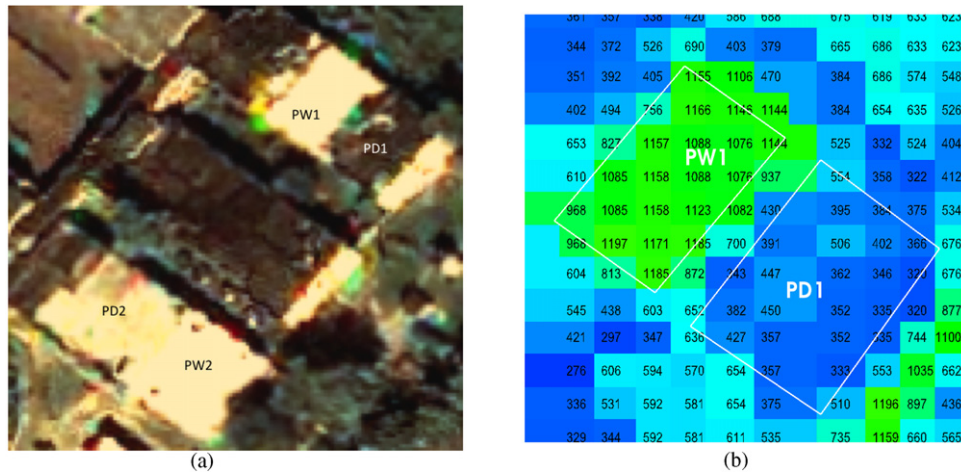


Figure 2. (a) True color image of light (PW1, PW2) and unpainted (PD1, PD2) roofs at the Pantnagar site taken on 21 October 2011. The roof labeled PD2 is considerably more reflective than PD1 but less reflective than PW2. All four roofs at Pantnagar are horizontal. (b) DNs for the NIR band at Pantnagar roofs PW1 (higher values in green) and PD1 (lower-valued dark blue pixels below and right of PW1).

Table 1. Metadata of the six IKONOS satellite data sets purchased in 2011 and 2012. Elevation is measured from the horizontal. Azimuth is measured clockwise from North. Cloud cover refers to the whole image extent, not merely the target roofs.

Imaging date	Location	Solar elev. (deg.)	Solar azim. (deg.)	IKONOS		% cloud cover	UTC time of acquisition
				elev. (deg.)	azim. (deg.)		
13 Oct. 2011	Nainital	50	155	64.6	30.1	0	05:26
21 Oct. 2011	Pantnagar	47.2	154.9	63.4	123.2	1	05:19
21 Dec. 2011	Nainital	35.5	163.2	63.1	241.6	0	05:41
26 Dec. 2011	Pantnagar	34.4	157.7	73.2	112.0	0	05:23
20 Mar. 2012	Nainital	53.7	139.3	64.2	80.5	1	05:19
20 Mar. 2012	Pantnagar	54.0	139.2	66.3	100.3	0	05:20

Table 2. Approximate TOA and surface energy content within the IKONOS band limits. The calibration coefficients C_k calculated in the IKONOS calibration study of Pagnutti *et al* (2003), and the band-averaged attenuation RSR_k are in columns 7 and 8 respectively.

Band	Low edge (μm)	High edge (μm)	Width (nm)	TOA (W m^{-2})	Surface (W m^{-2})	C_k ($\text{m}^2 \text{Sr W}^{-1}$)	RSR_k
Blue	0.445	0.516	71.3	140	114	72.8	0.79
Green	0.506	0.595	88.6	165	143	72.7	0.86
Red	0.632	0.698	65.8	101	93	94.9	0.85
NIR	0.757	0.852	95.4	109	104	84.3	0.74

the Indian towns of Nainital and Pantnagar were taken from a sun-synchronous near-polar orbit at altitude 680 km at approximately 1030 h local time (0530 h ahead of UTC). Two shots were taken in October 2011, two shots close to the winter solstice of 2011, and two shots on the spring equinox of 2012. Figure 2(a) shows one such shot, and table 1 lists details of all six shots.

The data set from each shot includes five images: a 1 m spatial resolution pan-chromatic image and four multi-spectral (MS) images in the blue, green, red and near-infrared (NIR) bands. Table 2 shows the band spectral extents, and the incident solar radiometric power contained in each band at the TOA and surface (estimated using a fairly clean representative atmosphere). The light intensity of each pixel has a dynamic range of 11 bits, from 0 to 2047, and the value is commonly referred to in the remote sensing

community as a digital number (DN_k) for each band, $k = \text{blue, green, red, NIR}$.

Digital number values recorded by IKONOS were converted to radiance at the telescope aperture $\text{W m}^{-2} \text{Sr}^{-1}$ using previously determined radiometric calibrations (Bowen 2002, Pagnutti *et al* 2003), and a correction for the spectral response of the IKONOS bands. During the IKONOS calibration study spectrally resolved radiometric measurements were made on the ground at the times of the overhead IKONOS transit. Using independently measured values of atmospheric transmissivity, and applying a radiative transfer model (RTM), the spectral radiance entering the satellite aperture, $L^{\text{ap}}(\lambda)$ in $\text{W m}^{-2} \text{Sr}^{-1}$, was calculated. Convoluting $L^{\text{ap}}(\lambda)$ with the relative spectral responses of the band-pass filters, $RSR_k(\lambda)$, they obtained the in-band radiance, L_k^{ib} , of each band, where $RSR_k(\lambda)$ were obtained

from pre-launch laboratory measurements of the band-pass filters. Calibration coefficients for each band, were then calculated as

$$C_k = DN_k / L_k^{ib}. \quad (1)$$

For our study we require L_k^{ap} , not L_k^{ib} , and normalize by the mean fractional attenuation of each filter, RSR_k , as

$$L_k^{ap} = (DN_k / C_k) / RSR_k \quad k = \text{blue, green, red, NIR}. \quad (2)$$

The average DN_k for each MS band and for each roof was calculated using a spatial analysis of each pan-chromatic image, because of its higher spatial resolution. The rooftop corner points are located and all pixels within these are initially taken as being on the roof. Figure 2(b) shows the DNs for rooftop pixels of the rooftop shown in figure 2(a) for the NIR band. Over a roof, the mean and standard deviation value of the rooftop pixel DNs is determined for each of the four MS bands. Outliers are discarded, which is effective at removing pixels that only partially cover the roof or contain chimneys and other structures. A pixel is tagged as an outlier if it differs by more than one standard deviation from the mean in all of the four bands or has a very large deviation in one or more bands. After outliers are discarded, the mean of each MS band is recalculated and the result is taken as being the DN_k value representative of the roof. This is then converted to a radiance using equation (2). The at-aperture radiance L_k^{ap} was then calculated from DN_k , using the calibration coefficients from table 2 and equation (2). Finally, for the purpose of comparing with the RTM, since the one-dimensional RTMs work in radiant emittance (units are $W m^{-2}$) rather than radiance, we multiply L_k^{ap} by π to convert radiance to radiant emittance, under the assumption that the roof can be approximated as a Lambertian reflector.

2.3. Radiative transfer model

The radiative transfer modeling is conducted using RRTMG_SW, based on the old RRTMG_SW (Mlawer *et al* 1997) scheme with an accuracy in clear sky within $3 W m^{-2}$ for flux at all levels, and heating rate agreement to within $0.1 K d^{-1}$ in the troposphere. The model covers the spectral range $820-50000 cm^{-1}$ ($0.2-12.2 \mu m$) (although 95% of the total downwelling energy at TOA is covered in the interval ($0.2-2.0 \mu m$)), provides good efficiency with minimal loss of accuracy for global climate model (GCM) applications, and is widely used in the modeling community. Molecular absorbers included are water vapor, carbon dioxide, ozone, methane and oxygen.

Air temperature, water vapor and O_3 profiles to drive the RRTMG_SW scheme were extracted from the Modern-Era Retrospective Analysis for Research and Applications (MERRA) product (a detailed overview can be found in Rienecker *et al* 2011) at a spatial resolution of $2/3^\circ \times 1/2^\circ$. The profiles cover the entire atmosphere from the surface to 0.01 hPa ($\sim 70 km$ asl) at a 6 h temporal frequency. Only the instantaneous values at 06:00 UTC were considered because

the IKONOS satellite images were taken at this time (between 05:00 and 06:00 UTC in both places, $LT = UTC + 05:30$).

The aerosol optical depth (AOD) and the mean surface albedo R_M are required to drive the model and they were retrieved from the moderate resolution imaging spectral radiometer (MODIS) on the Aqua satellite instrument with a spatial resolution of $10 km \times 10 km$ at nadir (MYD04.L2 product). The AODs at 0.47 and $0.55 \mu m$ were used to obtain the spectral dependence relation for the 14 bands considered in the RRTMG_SW scheme. Because of the unknown vertical distribution of the aerosol loads, a constant profile limited to the first $\sim 2.5 km$ above the ground was assumed. The R_M used in the runs was the mean value of the three surface albedos retrieved from the MODIS-Aqua instrument at $0.47, 0.55$ and $0.66 \mu m$ wavelengths.

In the radiative scheme the SW_{\downarrow} radiation has two components: direct and diffuse. In contrast to the direct component, the diffuse component has contributions from multiple reflections between the atmosphere and the surrounding areas. Consequently, the total $SW_{\downarrow SFC}$ flux cannot be computed using the surface albedo of the roofs, and the mean albedo R_M had to be considered instead. The performance of the RRTMG_SW was evaluated comparing the $SW_{\downarrow SFC}$ fluxes against the measurements on the roofs, and later the radiative model was compared with the IKONOS satellite computing the $SW_{\uparrow TOA}$ fluxes. The RRTMG_SW was called every two minutes during the half hour that includes the time of the IKONOS acquisition (see table 1) and the fluxes were averaged.

The calculation of the fluxes reflected to space from the roofs $SW_{\uparrow TOA}$ requires a different procedure (see section 2.3.1) than just running the model. Thanks to the inter-comparison with IKONOS, the robustness of this procedure could be evaluated. Only particular bands were considered in the inter-comparison because the partitionings of the shortwave spectrum into bands by the RRTMG_SW and the satellite instrument were somewhat different. The blue ($0.445-0.516 \mu m$) plus green ($0.506-0.595 \mu m$) IKONOS bands were extrapolated to cover completely band 10 ($0.442-0.625 \mu m$) of the RRTMG_SW scheme with a simple extrapolation. The high spatial resolution of IKONOS permits us to estimate the different fluxes at TOA coming from each individual roof.

2.3.1. $SW_{\uparrow TOA}$ derived with the RRTMG_SW scheme. As previously commented, the RRTMG_SW could not be used with the albedo of the roofs to compute the $SW_{\uparrow TOA}$ fluxes because undesirable errors are introduced in the diffuse component of the $SW_{\downarrow SFC}$. To avoid this setback, the following procedure was adopted. Let us consider the atmosphere like a single layer over the ground (some years ago Rassel and Schneider (1971) used this concept to describe a layer of aerosols), and let t and r be the transmission and reflection of this layer (in this context t and r are exclusively properties of the atmosphere). With the help of the RRTMG_SW scheme, these two parameters can be computed assuming that the ground surface is totally absorbing

($R_M = 0$):

$$t = \frac{SW_{\downarrow SFC}}{SW_{\downarrow TOA}} \Big|_{R_M=0} \quad (3)$$

$$r = \frac{SW_{\uparrow TOA}}{SW_{\downarrow TOA}} \Big|_{R_M=0} \quad (4)$$

Now, the effect of the atmosphere can be described in a way that permits us to compute the fluxes at TOA when we are ‘looking’ a particular roof from space. To avoid loss of energy, let us permit that the rays coming from the Sun can be reflected infinite times over the ground when they cross the atmosphere. The first reflection (that takes place over the roof) would represent the ‘direct’ component of the radiation and the rest of the infinite reflections (over the surrounding areas) would represent the ‘diffuse’ component of the total radiation that reaches our ‘eyes’. In this model, each time that a ray crosses the atmosphere it suffers a reflection r and a transmission t , and consequently the $SW_{\uparrow TOA}$ can be computed as the sum of the following geometrical series:

$$r + t^2 R_R \sum_{n=0}^{+\infty} r^n R_M^n = r + \frac{t^2 R_R}{1 - r R_M} = \frac{SW_{\uparrow TOA}}{SW_{\downarrow TOA}} \quad (5)$$

where R_R is the albedo of the roof and R_M the mean albedo of the surrounding areas. The model of the infinite reflections permits us to describe the effect of the atmosphere on the shortwave radiation. Part of the energy of a ray is backscattered, part is absorbed, and the rest is transmitted. At the ground, part is absorbed and the rest is reflected, so repeating this process infinite times the energy can be conserved. For the inter-comparison with the IKONOS values, the $SW_{\uparrow TOA}$ for the different roofs was computed using equation (5) (the $SW_{\downarrow TOA}$ was restricted to band 10 just like the right terms in the previous equations (3) and (4)), and only the transmission t and reflection r parameters were derived with the RRTMG_SW scheme. Previous to the inter-comparison and to be sure that equation (5) works correctly, the $SW_{\uparrow TOA}$ with the RRTMG_SW (fixing the surface albedo to R_M) was compared against equation (5) (with $R_R = R_M$) and the fluxes matched 98–99% in all the cases analyzed.

3. Results and discussion

3.1. Results

Measured downwelling shortwave fluxes from ground-based radiometers, $SW_{\downarrow SFC}$, are shown together with AOD at $0.55 \mu m$ from MODIS, and predictions of $SW_{\downarrow SFC}$ from RRTMG_SW for the time of IKONOS observations in table 3. The radiative transfer model was able to reproduce the surface fluxes (the absolute mean bias was $10.49 W m^{-2}$ once the AOD values were modified), but the differences between measured and default (without aerosols) RRTMG_SW results for $SW_{\downarrow SFC}$ can vary by up to $\sim 250 W m^{-2}$, demonstrating the importance of the aerosol loads. Except for two days, the AOD values considered in the runs (column 8) were

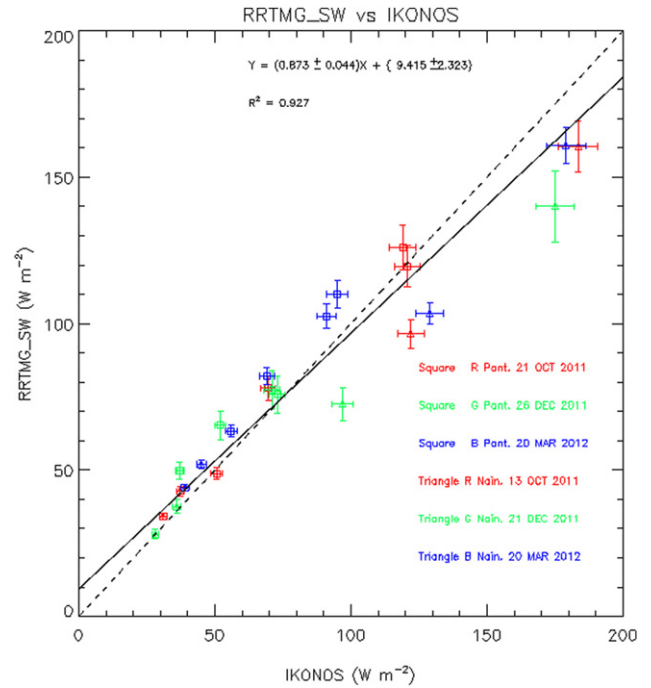


Figure 3. Scatter plot RRTMG_SW(band 10) versus IKONOS (B + G extrap.) showing the computed $SW_{\uparrow TOA}$ fluxes. The bars represent the range of uncertainty of the values.

generally higher than the values retrieved from MODIS. One likely source of the discrepancies is that local aerosol sources near the Pantnagar site were not resolved by the 10 km MODIS imaging. However, we cannot uniquely identify this as the cause. Equation (5) was then used to estimate the atmospheric transmission and reflection (t and r), which differed between Nainital and Pantnagar. The transmission and reflection differences between the two sites are likely due to differences in the vertical profiles of aerosol concentration, and the season dependence of the path ray lengths. In particular, the AOD values for Pantnagar were greater than the values for Nainital (see, e.g., Sagar et al 2004). Approximately 80–90% of band 10 was transmitted $t/(1 - rR_M)$ at Nainital, whereas only 60–75% reached the ground at Pantnagar.

Surface measured SW roof albedo and upwelling fluxes at TOA, $SW_{\uparrow TOA}$, are reported in table 4 for each of the dates with IKONOS observations. In all cases, higher values of $SW_{\uparrow TOA}$ are obtained for the white roofs at each site (column 3), with light and dark roofs ranging from 40 to $400 W m^{-2}$, depending on the site and season. Moreover, comparison of satellite observations and modeled values of $SW_{\uparrow TOA}$ show a strong ($R^2 = 0.927$) linear dependence in figure 3, demonstrating that RRTMG_SW accurately predicts the increase in $SW_{\uparrow TOA}$ for reflective roofs in aerosol rich atmospheres. In addition, the ratio of band 10 to total radiative flux from IKONOS (B + G + R + NIR) is approximately constant (0.50 ± 0.04) for all the roofs and dates, suggesting that equation (5) could be used covering the entire shortwave spectrum to estimate the total energy at TOA when satellite measurements were not available.

Owing to the different orientation of the roofs at Nainital, the surface albedos on the white roofs (NW1 and

Table 3. Measured and computed surface and atmospheric properties, and downwelling SW radiation for dates and times of IKONOS observations.

Imaging date	R_M	AOD 0.55 μm (MODIS)	$\text{SW}_{\downarrow\text{SFC}}$ (measured) (W m^{-2})	$\text{SW}_{\downarrow\text{SFC}}$ (computed w/o AOD) RRTMG (W m^{-2})	Transmission t (computed)	Reflection r (computed)	AOD 0.55 μm (computed)
13 Oct. 2011 (N)	0.104	0.331	802.53 \pm 22.19	817.17 \pm 14.65	0.864 \pm 0.040	0.088 \pm 0.004	0.145
21 Oct. 2011 (P)	0.165	0.626	637.35 \pm 22.73	759.88 \pm 14.30	0.718 \pm 0.042	0.154 \pm 0.009	0.626
21 Dec. 2011 (N)	0.140	0.092	665.90 \pm 35.90	675.71 \pm 10.29	0.874 \pm 0.061	0.088 \pm 0.006	0.092
26 Dec. 2011 (P)	0.126	0.080	472.43 \pm 31.34	614.94 \pm 13.90	0.641 \pm 0.059	0.203 \pm 0.019	0.578
20 Mar. 2012 (N)	0.096	0.269	826.25 \pm 14.22	916.95 \pm 15.03	0.800 \pm 0.029	0.113 \pm 0.004	0.445
20 Mar. 2012 (P)	0.149	0.762	639.35 \pm 16.79	906.57 \pm 14.93	0.586 \pm 0.028	0.190 \pm 0.009	1.484

Table 4. Seasonal variation in roof surface albedo and shortwave fluxes at TOA. The values in column 3 and 4 have been corrected to take into account gaps and overlaps between the IKONOS bands.

Roofs	$\alpha \equiv \frac{\text{SW}_{\uparrow\text{SFC}}}{\text{SW}_{\downarrow\text{SFC}}}$ (surface)	IKONOS (TOA) B + G + R + NIR (W m^{-2})	IKONOS (TOA) band 10 (W m^{-2})	RRTMG_SW (TOA) Band 10 (W m^{-2})	$\left(\frac{\text{RRTMG_SW}}{\text{IKONOS}}\right)_{\text{Band10}}$ (TOA)
13 Oct. 2011 (Nainital)					
NW1	0.38	248	122	97	0.79
NW2	0.71	387	183	160	0.88
ND1	0.06	57	31	34	1.10
ND2	0.10	73	37	43	1.15
21 Oct. 2011 (Pantnagar)					
PW1	0.62	262	121	120	0.99
PD1	0.08	95	51	49	0.97
PW2	0.67	261	119	126	1.06
PD2	0.30	144	70	78	1.12
21 Dec. 2011 (Nainital)					
NW1	0.34	196	97	72	0.75
NW2	0.76	382	175	140	0.80
ND1	0.06	45	28	28	1.00
ND2	0.12	70	36	38	1.04
26 Dec. 2011 (Pantnagar)					
PW1	0.42	155	73	76	1.04
PD1	0.11	66	37	50	1.34
PW2	0.44	149	71	77	1.09
PD2	0.30	104	52	65	1.26
20 Mar. 2012 (Nainital)					
NW1	0.39	260	129	104	0.80
NW2	0.70	381	179	161	0.90
ND1	0.07	69	39	44	1.13
ND2	0.11	87	45	52	1.15
20 Mar. 2012 (Pantnagar)					
PW1	0.49	194	91	103	1.13
PD1	0.10	106	56	63	1.13
PW2	0.56	204	95	110	1.16
PD2	0.28	141	69	82	1.19

NW2) were different for each of the dates of the IKONOS observations. Only the untreated roofs showed no significant differences. However, the white roofs at Pantnagar (PW1 and PW2) presented similar albedos although they suffered slight degradation due to natural soiling and/or weathering processes during the campaign.

3.2. Discussion

Considering the entire shortwave spectrum to gauge the attenuation of the atmosphere, the effective albedo α of the earth-atmosphere system can be calculated using equation (5). Differentiating this expression, we obtain the

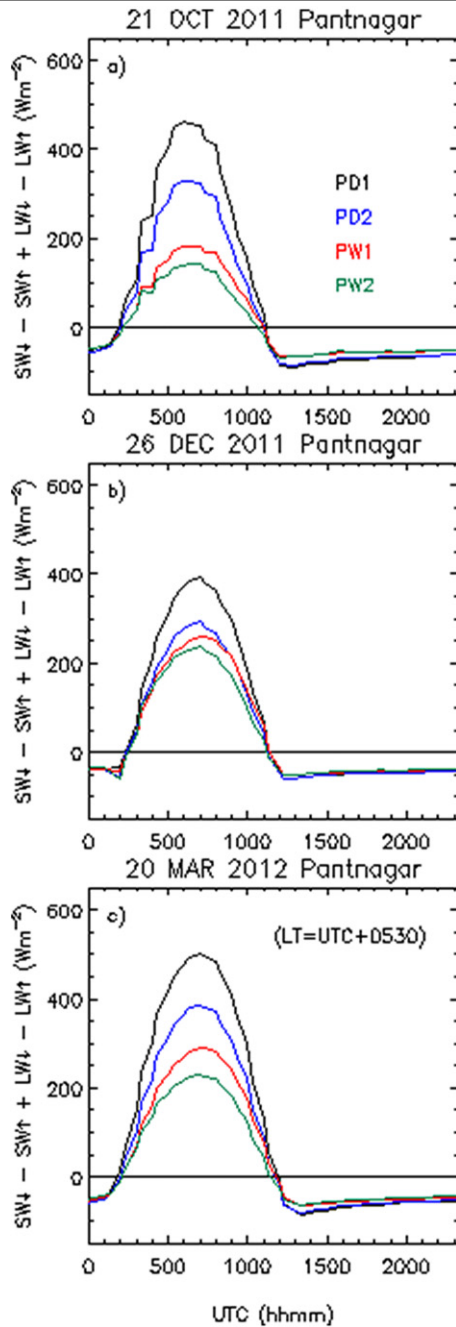


Figure 4. Daily net all-wave radiation (urban energy balance) on Pantnagar. Positive values mean a net energy absorbed into the roof, negative values mean net energy emitted and reflected from the roof.

response to a change in the surface albedo R_R :

$$\frac{d\alpha}{dR_R} = \frac{t^2}{1 - rR_M} \approx t^2. \quad (6)$$

Equation (6) shows that the effectiveness of the reflective cool surfaces depends on the atmospheric transmissivity. Clean environments are more effective than polluted environments. The same equation can be written in terms of the net shortwave benefit $\Delta SW_{\uparrow TOA}$ when the albedo is modified by a quantity ΔR_R :

$$\Delta SW_{\uparrow TOA} = SW_{\downarrow TOA} \frac{t^2}{1 - rR_M} \Delta R_R. \quad (7)$$

In our case, the mean benefit $\Delta SW_{\uparrow TOA}$ for the six shots was $48.66 \pm 11.63 \text{ W m}^{-2}$ for each $\Delta R_R = 0.1$ increase of the albedo when the entire spectrum was considered. Obviously this magnitude would have been different with different atmospheric conditions or at different times. To estimate the benefit globally a complete annual analysis should be carried out, covering the whole campaign. As a first approximation, considering a transmission of $t = 0.7$ and a daily mean solar insolation typical of March at these latitudes ($\sim 400 \text{ W m}^{-2}$), we would obtain a daily mean benefit of $\sim 20 \text{ W m}^{-2}$ for each 0.1 increase of the albedo.

When the albedo of a roof is increased, the surface absorbs less solar energy and its temperature (T_R) decreases; consequently, the longwave emission ($\propto T_R^4$) can be reduced significantly relative to the dark (hotter) roof. To take into account the effect of the longwave radiation, the net all-wave radiation was analyzed. Figure 4 shows the measured net all-wave radiation (urban energy balance) $SW_{\downarrow} - SW_{\uparrow} + LW_{\downarrow} - LW_{\uparrow}$ just above the roofs on Pantnagar. The urban energy balance (Oke 1988) represents the energy available (together with any possible source of anthropogenic heat) that is partitioned in sensible, latent and storage heat fluxes in an urban canyon. A positive value means a net gain and a negative value a net loss of energy in the urban surface. Looking at figure 4, it is clear that the reflective cool roofs (PW1, PW2) showed a mean daily benefit because the values were lower (less heat gain) than for dark roofs during the day, and had similar values during the night. The maximum differences were observed between the PD1 and PW2 roofs, and showed significant season dependence. The differences reached up to 350, 200 and 300 W m^{-2} on 21 October, 26 December and 20 March, respectively. Although the surface temperatures were not directly monitored during the campaign, the longwave radiation captures the radiant effect of having different surface temperatures for the light and dark surfaces such that the mean benefit of the white roofs remains significant but not important during the night (see, e.g., Gaffin *et al* 2012).

Similar conclusions were derived on Nainital⁷ (not shown on figure). Except the ND1 roof, the rest of the roofs did not present energy differences during the night. At Nainital the roofs sloped slightly: ND1 and NW1 faced northwest and ND2 and NW2 faced southeast; consequently, the temporal evolution of the net radiation balance differed depending on the orientation. The urban energy balance peaked at $\sim 0530\text{--}0600$ UTC at ND1 and NW1, while peaked at $\sim 0900\text{--}0930$ UTC above the other two roofs. On Pantnagar, all the roofs were horizontal, hence their radiation balances peaked at the same time (~ 0700 UTC).

4. Conclusions and future work

This work demonstrates that reflective roofs are effective in reflecting an important fraction of solar radiation back to space even in atmospheres with significant aerosol loading,

⁷ A figure showing the urban energy balance on Nainital is available as supplementary material available at stacks.iop.org/ERL/7/044007/mmedia.

and that the RRTMG_SW model captures this radiative benefit, but is sensitive to the aerosol loads. Results show a mean increase of $\sim 50 \text{ W m}^{-2}$ outgoing at TOA for each 0.1 increase of the urban albedo at the time of the observations. In principle, to estimate the benefits globally, the RRTMG_SW could be combined with atmospheric properties from MERRA and MODIS to conduct a study of the annual-average effectiveness, that could include the effect of clouds. Beyond site-specific evaluation, a high-resolution study coupling radiation and clouds would also be useful for improving our understanding of the globally averaged benefits of white roofs for climate change mitigation.

Acknowledgments

We gratefully acknowledge Professor Ram Sagar and Dr Rao Kotamarthi for advice and assistance in arranging fieldwork at Nainital as part of the RAWEX-GVAEX campaign and the useful comments of two reviewers. We also thank Bipin Shah (Winbuild) for arranging the roof coatings, Ken Reichl for assistance with radiometer instrument preparation and initial data reduction, and Jyotirmay Mathur and Jaipur J Niranjana for assistance with data collection in the field. This work is supported by the US DOE Office of Energy Efficiency and Renewable Energy, and the US DOE Office of Science, Atmospheric Radiation Measurement program, under contract DE-AC02-05CH11231.

References

Bowen H S 2002 Absolute radiometric calibration of the IKONOS sensor using radiometrically characterized stellar sources

- Pecora 15/Land Satellite Information IV/ISPRS Commission I/FIEOS 2002 Conf. Proc.*
- Gaffin S R, Imhoff M, Rosenzweig C, Khanbilvardi R, Pasqualini A, Kong A Y Y, Grillo D, Freed A, Hillel D and Hartung E 2012 Bright is the new black—multi-year performance of high-albedo roofs in an urban climate *Environ. Res. Lett.* **7** 014029
- Iacono M J, Delamere J S, Mlawer E J, Shephard M W, Clough S A and Collins W D 2008 Radiative forcing by long-lived greenhouse gases: calculations with the AER radiative transfer models *J. Geophys. Res.* **113** D13103
- IKO1 1999 www.satimagingcorp.com/satellite-sensors/ikonos.html
- Menon S, Akbari H, Mahanama S, Sednev I and Levinson R 2010 Radiative forcing and temperature response to changes in urban albedos and associated CO₂ offsets *Environ. Res. Lett.* **5** 014005
- Millstein D and Menon S 2011 Regional climate consequences of large-scale cool roof and photovoltaic array deployment *Environ. Res. Lett.* **6** 034001
- Mlawer E J, Taubman S J, Brown P D, Iacono M J and Clough S A 1997 Radiative transfer for inhomogeneous atmospheres: RRTM, a validated correlated-*k* model for the longwave *J. Geophys. Res.* **102** 16663–82
- Oke T R 1988 The urban energy balance *Prog. Phys. Geogr.* **12** 471–508
- Pagnutti M, Ryan R E, Kelly M, Holekamp K, Zanoni V, Thome K and Schiller S 2003 Radiometric characterization of IKONOS multispectral imagery *Remote Sens. Environ.* **88** 53–68
- Rassol S I and Schneider S H 1971 Atmospheric carbon dioxide and aerosols: effects of large increases on global climate *Science* **173** 138
- Rienecker M M *et al* 2011 MERRA: NASA's modern-era retrospective analysis for research and applications *J. Clim.* **24** 3624–48
- Sagar R, Kumar B, Dumka U C, Krishna Moorthy K and Pant P 2004 Characteristics of aerosol spectral optical depths over Manora Peak: a high-altitude station in the central Himalayas *J. Geophys. Res.* **109** D06207